RSC Advances

This is an *Accepted Manuscript*, which has been through the Royal Society of Chemistry peer review process and has been accepted for publication.

Accepted Manuscripts are published online shortly after acceptance, before technical editing, formatting and proof reading. Using this free service, authors can make their results available to the community, in citable form, before we publish the edited article. This *Accepted Manuscript* will be replaced by the edited, formatted and paginated article as soon as this is available.

You can find more information about *Accepted Manuscripts* in the **Information for Authors**.

ROYAL SOCIETY OF CHEMISTRY

www.rsc.org/advances

Layer-by-layer deposition of CNT^- and CNT^+ hybrid films for platinum free counters electrodes of dye-sensitized-solar-cells

Majid Raissan Al-bahrani,[1,2] Waqar Ahmad[1], Shi-Sen Ruan[3], Zhichun Yang[1] Ze Cheng[4] and Yihua Gao[1],*

[1]Center for Nanoscale Characterization & Devices (CNCD), Wuhan National Laboratory for Optoelectronics (WNLO), School of Physics, Huazhong University of Science and Technology (HUST), Wuhan,   Hubei 430074, P.R. China.

[2]Faculty of Computer Science and Mathematics, Thi-Qar University, Nasiriyah, Iraq.

[3]Hubei University Science and Technology, School of Electronic and Information Engineering, 437100, P.R. China.

[4]School of Physics, HUST, Wuhan,   Hubei 430074, P.R. China.

* Corresponding author. Tel. / Fax: 0086 15807135274 -0086 27 87793877.

E-mail address: gaoyihua@hust.edu.cn

Abstract

A nanocomposite film of polyaniline blend poly (sodium 4-styrenesulfonate)/ multiwall CNT (PANI-PSS/MWCNT) and poly (diallydimethyl ammonium chloride)/ multiwall CNT (PDADMAC/MWCNT) has been prepared as a highly-efficient catalytic material for the counter electrode (CE) of dye-sensitized solar cell (DSSC). The as-prepared CE is constructed by a nanoscale method of layer-by-layer (LbL) assembly based on the electrostatic interactions between negatively (PANI-PSS/MWCNT) and positively (PDADMAC/MWCNT) charged nanoparticles. The $(CNT^-/CNT^+)_4$ multilayer CE displayed remarkably enhanced electrocatalytic activities toward reduction reaction and low charge-transfer resistance (R_{ct}) of 0.3 Ω at the CE/electrolyte interface. The DSSC with $(CNT^-/CNT^+)_4$ multilayer-CE showed highest fill factor (0.71) and cell efficiency (9.13%) compared to our other electrodes.

.

1- Introduction

Nowadays, energy conversion devices have attracted receiving attentions due to their great potentials as power sources like dye-sensitized solar cells (DSSCs). As an alternative to silicon solar cells, DSSCs are considered to be low cost and environment friendly. DSSC mainly consists of dye sensitized photoanode, a redox mediator of I^-/I_3^- and counter electrode (CE) [1-3]. To improve the performance of DSSCs, much efforts did for each of the constituent components, including photoanode [4], dye molecules[5], electrolytes [6] and CE [7]. In typical DSSCs, the CE play crucial role for achieving a high performance i.e. excellent electrocatalytic ability and high conductivity. Due to their dual role, CE transport quickly electrons from electrode substrate to the electrolyte and effectively catalyzed the iodide-triiodide (I^-/I_3^-) redox reaction in the electrolyte. Platinum (Pt) is well-known noble metal and utilized as CE material for DSSCs. However, there are also shortcomings of using Pt, *i.e.* highly expensive and scarcity as a precious metal. Extensive studies have been made on Pt alternatives as the catalytic materials for the CEs of DSSCs, including conductive polymers [8-12], inorganic metal compounds [13], carbon-based materials [14-18], and composite materials [19]. Notably, carbon based materials have shown efficient performance and achieved significant improvement since last few years including graphene[16], nanocarbon [17, 18], carbon black [20], activated carbon[21], single-walled carbon nanotube (SWCNT) [22], and multi-walled carbon nanotube (MWCNT) [23] *etc*.

Since 1991 [24], CNTs attracted a tremendous attentions due to their unique nanostructure and fascinating properties like high conductivity, high chemical

stability, good catalytic ability and low-cost. Choi et al. prepared CNTs CE by screen printing technique and showed efficiency of 5.94% [25]. Ramasamy et al. describe the use of spray coated multi-wall CNTs on FTO glass substrate as CEs for I_3 reduction with an efficiency of 7.59% [23]. To enhance the electrocatalytic activity of CNTs, Lee et al. reported CNTs based CE by doctor blade method [26] which showed an enhanced photovoltaic performance (7.7%). There are other methods used for manufacture CEs such as chemical vapor deposition [27]. Recently, studies focused on the chemical deposition, electrode position, and spin-coating of graphene/polyaniline composite [28], carbon fiber/PEDOT: PSS [29], graphene/polyaniline hybrid [30] *et al*. Typically, in CEs of DSSCs, the interfacial resistance between conducting polymer and carbon material is relatively high because of their weak bonding which gives low charge-transfer kinetics. To control over the CNTs assembly in thin films, the layer-by-layer (LBL) technique was used in multilayers [31], where positive and negative layers banded with each other [32].

In this paper, we prepared a new CE for DSSCs, prepared by LBL concept of negatively charged PANI-PSS/MWCNT (anionic) and positively charged PDADMAC/MWCNT (cationic) by polyelectrolyte multilayers technique. The obtained power conversion efficiency (PCE) of our prepared $(CNT^-/CNT^+)_4$ multilayer-CE based DSSC is 9.13% under AM 1.5G simulated solar irradiation of 100 mW/cm^2. Notably, the variation in the thickness towards the fabrication of CNT^-/CNT^+ nanocomposite film significantly accelerates the overall PCE of the DSSC. Moreover, the superior performance $(CNT^-/CNT^+)_4$ multilayer-CE is the

cost-effective way for highly efficient CEs of DSSCs.

2- Experimental details

Materials and device fabrication

To prepare the CEs of DSSCs, we utilize LBL technique of polyelectrolyte self-assembly as shown in Scheme 1. MWCNTs were dispersed with cationic or anionic polyelectrolytes. First, the anionic PANI-PSS was synthesized by previously reported literature [33]. In detail, MWCNTs (5 mg) were mixed with a solution of 100 ml solution of PANI-PSS content with weight concentration 0.15% (w/w). To attain the homogeneous suspension, the mixed solution was ultrasonicated in an ice bath for 60 min. Second, the preparation of cationic MWCNTs modified with PDADMAC was done by mixing 5 mg of MWCNTs in 100 mL of PDADMAC content with concentration of weight 0.16% (w/w). The solutions were stirred and sonicated for 60 min. Finally, these solutions were used for LBL self-assembly to make the CNTs into thin films deposited on the surface of a cleaned fluorinated tin oxide (FTO, 15 Ω/cm^2, 90% transmittance in the visible light, Nippon Sheet Glass Co.) glass by dip coating method. To achieve multilayered films the FTO glass was dipped sequentially in solutions of cationic and anionic. For the generation of positively charged and strong adhesion of CNTs on FTO glass, we coated 6 layers of PDADMAC-PSS on FTO substrate. Then the first layer of anionic PANI-PSS/MWCNT was deposited by simply dipping the as-prepared sample into a PANI-PSS/MWCNT solution. The next layer of cationic PDADMAC/MWCNT also transferred onto the substrate by dipping the sample into a PDADMAC/MWCNT solution. The alternate LBL films of each positive and negative charge polyelectrolytes were achieved by repeating this process

until the desired number of layers was achieved. Afterwards, the films were dried in a stream of nitrogen and stored as depicted in Fig 1.

The working electrodes (WEs) were made of TiO_2 LBL hierarchical nanosheets (TiO_2 LHNs) paste by doctor blading. The TiO_2 LHNs was fabricated by the previously reported method [34]. Then the TiO_2 LHNs paste was prepared according to the previously paper [35], the TiO_2 LHNs powder (0.9 g) was added to the solution containing ethanol/water (4/1 mL), and acetylacetone (0.16 mL) under vigorously stirring for 3 h. Then, the prepared TiO_2 paste was applied on pre-treated FTO glass by doctor-blade method and sintered at 500 ºC for 30 min to achieve crystallization using a muffle furnace. After that, TiO_2 films with a thickness of 10 μm were sensitized in a N719 dye solution (0.5mM in 1:1 ethanol and acetonitrile solution) for at least 12 h at 60 °C in a sealed beaker. Afterwards, the WE was assembled. After an electrolyte (0.05 M I2, 0.1 M LiI (Adamas-beta), 0.6 M 1 methy l-3-butylimidazolium iodide (TCl), 0.1Mguanidiniumthiocyanate (TCl), and 0.5 M 4-tert-butylpyridine (TCl) mixed in 3-methoxypropionitrile solution (Alfa Aesar)) was filled, the J-V performance of the DSSCs was investigated using a solar-simulator illumination (Newport, USA).

3- Results and discussion

Material characteristics

The high resolution transmission and   scanning electron microscopy image of the PANI-PSS/MWCNT, PDADMAC/MWCNT and $(CNT^-/CNT^+)_n$ multilayer view of DSSCs prepared in this work is shown in Fig.2. Pristine MWCNTs are hollow multiwall objects including an outer diameter of 10-20 nm. The LBL deposition of nanoparticles into thin films, adequate electrostatic charges must be present at their surface for stable adsorption. Therefore, pristine MWCNTs need to be modified with either cationic or anionic polyelectrolytes before deposition for example PDADMAC and PANI-PSS in this paper. TEM images in Fig. 2a and b shows a uniform coverage of PDADMAC (3.3 nm) layer over the randomly distributed MWCNT network. While images in Fig. 2c and d clearly shown the PANI-PSS (9.5nm) formation around the surface of the MWCNTs. PANI-PSS was used to improve the adsorption of the MWCNTs into multilayer thin films [36]. The SEM image Fig.2e depicts the morphology of deposited films which discloses a uniform coverage.

Multilayer preparation can enhance the absorbance, as shown in Fig. 2f, the UV/Vis absorbance spectra. The inset Fig 2f shows that the $(CNT^-/CNT^+)_n$ layers is morphologically homogeneous in all aspects. The $(CNT^-/CNT^+)_n$ spectrum contains a strong absorption band at 750 nm, due to the polyaniline in the films PANI-PSS as polyelectrolytes versus PANI/PSS used to modified the MWCNTs and also all $(CNT^-/CNT^+)_n$ multilayer display an increase in absorbance with the wavelength.

Fig 2f shows the maximum absorption occur ~750 nm for all four samples and the

intensity of this peak has been increased with the number of $(CNT^-/CNT^+)_n$ multilayer.

Electrocatalytic and electrochemical characteristics

The electro-catalytic activity of the CEs was evaluated via cyclic voltammetry (CV) for the reduction of triiodide ions in detail. Fig. 4a shows cyclic voltammograms of the four-electrode electrochemical cell based of $(CNT^-/CNT^+)_n$ multilayer CEs toward redox reactions of iodide/triiodide species. The oxidation of iodide happens at the photo electrode and the reduction of triiodide occurs at the counter electrode, which are ascribed to the redox reaction of I_3^- + 2e→3I^- [37]. In DSSC based of $(CNT^-/CNT^+)_4$ multilayer CE, a pair of oxidation (3.083 eV) and reduction (-4.079 eV) peaks are detected. The peak positions and shapes of the $(CNT^-/CNT^+)_n$ CEs, affecting the DSSC performances as shown in Fig. 4b and c. Therefore, the electro-catalytic activity for the $(CNT^-/CNT^+)_4$ CE appears to be the best, in which its catalytic current density is the highest. Additionally, Fig. 4d clearly shows that the $(CNT^-/CNT^+)_4$ CE displays a smaller peak-to-peak separation (E_{pp}) value than others, indicating a faster charge transfer kinetics than reference CEs under the same experimental condition [38]. The high current density of $(CNT^-/CNT^+)_4$ may be attributed to its layered structure. Notably, the multilayer films display more layered structure for I^-/I_3^- transportation and redox reactions, giving a faster reaction kinetics for iodide [38]. For comparison study we also prepared Pt electrodes by deposition of ca. 20μL/cm^2 of H_2PtCl_6 solution (2 mg of Pt in 1 mL of ethanol) and sintered at 400 °C for 15 min as shown in Fig. 6a. The peaks current density and E_{pp} of both

electrodes are shown in Fig. 6b. The $(CNT^-/CNT^+)_4$-CE achieves highest current

density with smaller E_{pp} to that of Pt-CE. The smaller E_{pp} is more effective to

improve the catalytic activity of CEs. The enhanced current density and decreased E_{pp}

values suggests that $(CNT^-/CNT^+)_4$-CE has good catalytic activity, which might be

the main reason for improved electrocatalytic performance of DSSCs.

In general, DSSCs have a diode-like element; the simple equivalent circuit consists of

the current source, diode, capacitances, and the resistances. The relationship between

current I and the voltage V at its terminals is given by

$$I_o = I_{PH} - I_D - I_{SH} \tag{1}$$

In other words, the output current I_o is calculated by

$$I_o = I_{PH} - I_0\{\exp(q\frac{V + IR_T}{nkT}) - 1\} - \frac{V + IR_T}{R_{SH}} \tag{2}$$

$$where \qquad I_D = I_0\{\exp(q\frac{V + IR_T}{nkT}) - 1\}, \quad I_{SH} = \frac{V + IR_T}{R_{SH}}$$

where, I_0, V, q, n, T, k and R_{SH} are dark saturation current of the diode, voltage,

elementary charge, ideality factor, temperature, Boltzmann constant and shunt

resistance through the back electron transfer, respectively.

In order to obtain additional information about the resistance of the DSSC based

$(CNT^-/CNT^+)_n$-CE, electrochemical impedance spectroscopy (EIS) was employed.

Typically, Nyquist plot consists of two or three semicircles. The intercept of first

semicircle on real axis in high frequency range (10^6 to 10^5 Hz) represents series

resistance (Rs) which is related to FTO sheet resistance, contact resistance and

external circuit resistance. The charge transfer resistance (R_{ct}) at the

electrode/electrolyte interface relates to the intrinsic catalytic properties of the counter

electrode materials for the reduction of I_3^- to I^- [39]. The DSSC fabricated with the

$(CNT^-/CNT^+)_n$-CE (n =1, 2, 3 or 4) and $(CNT^-/CNT^+)_4$-CE was measured to compare the performance of $(CNT^-/CNT^+)_n$-CE (n=1, 2 or 3) (Fig. 5a). The R_{ct} decreased clearly from $(CNT^-/CNT^+)_1$ to $(CNT^-/CNT^+)_4$-CE as shown in Fig. 5b-c. The redox reaction resistance (R_{ct}) of the CE affects the FF and PCE of cells in a negative way [38, 40, 41]. Therefore, DSSC device using the $(CNT^-/CNT^+)_4$-CE exhibits better performances than those of $(CNT^-/CNT^+)_n$ (n=1, 2 or 3)-CE, showing an elevated electrocatalytic activity at higher bilayers[42, 43]. The comparative EIS analysis curves of $(CNT^-/CNT^+)_4$ and Pt-CE are shown in Fig.6c. It can be seen that the R_{ct} of the as-prepared $(CNT^-/CNT^+)_4$-CE (0.3 Ω) is lower than that of the Pt-CE (0.7 Ω), which indicates the superior catalytic activity of $(CNT^-/CNT^+)_4$ that it has. The EIS results are in good agreement CV data.

The photocurrent density-voltage (*J-V*) characteristics of DSSCs based on $(CNT^-/CNT^+)_n$ multilayer CE were tested under 100 mW cm^2 AM 1.5 G illumination, using a black metal mask with the active cell area of 0.15 cm^2 as shown in Fig. 3a. All experimental curves are shown in Fig. 3b and their relative photovoltaic parameters are summarized in Table 1. As the number of (CNT^-/CNT^+) CE increased to four layers, the PCE is increased, because of high photocurrent density (J_{sc}). The enhanced efficiency is attributed to the elevated interfacial area in $(CNT^-/CNT^+)_4$ multilayer CE, which can accelerate the triiodide recovery and therefore promote electron-transfer kinetics. In a related context, the detailed PV parameters of the devices are shown in Table 1. The light-to-electric PCE and FF were calculated according to the equations [38]:

$$FF = \frac{V_{max} \times J_{max}}{V_{oc} \times J_{sc}} \qquad (3)$$

$$PCE = \frac{V_{max} \times J_{max}}{P_{in}} \times 100\% = \frac{V_{oc} \times J_{sc} \times FF}{P_{in}} \times 100\% \qquad (4)$$

where V_{max} and J_{max} are the voltage and the current density under the maximum power output in the J-V curves, respectively, J_{sc} is the short-circuit current density (mA/cm^2), V_{oc} is the open-circuit voltage (V), and P_{in} is the incident light power. The solar cells employing $(CNT^-/CNT^+)_4$ multilayer CEs showed highest efficiency of 9.13%, as compare to $(CNT^-/CNT^+)_3$, $(CNT^-/CNT^+)_2$ and $(CNT^-/CNT^+)_1$ bilayer showed PCE of 8.43%, 7.79% and 7.51%, respectively. The obtained data clearly demonstrate that employing $(CNT^-/CNT^+)_4$ multilayer CEs achieved high performance for solar cells. The comparative current density-voltage curves of $(CNT^-/CNT^+)_4$ and standard Pt CEs based DSSCs are shown in Fig. 6d. Table 1 shows the DSSC device performances with $(CNT^-/CNT^+)_4$ and Pt-CE, the solar cell fabricated with $(CNT^-/CNT^+)_4$-CE has achieved the PCE 9.13%, J_{sc} of 18.03 mA cm^{-2} and FF of 0.71%, which were better to the cell with Pt CE 8.40%, 17.16 mA cm^{-2} and 0.68%, respectively. The enhancement in J_{sc} and FF leading the DSSCs PCE performance is high.

4- Conclusions

In this work, we fabricated $(CNT^-/CNT^+)_n$ multilayer CEs in DSSCs by a LBL technique. The $(CNT^-/CNT^+)_4$ CEs exhibited good electrocatalytic performance for the redox couple and specific lower charge transfer resistance (R_{ct}) values at the CE/electrolyte interface. The $(CNT^-/CNT^+)_4$ device-based DSSC displayed the highest values of PCE (9.13%) and FF (0.71), which could be attributed to the low R_{ct} at the $(CNT^-/CNT^+)_4$-CE/electrolyte interface. The LBL method offers a novel easy synthesis, versatile electrical and photovoltaic performances for excellent CE material of DSSCs.

5- References

[1] B.O. Regan, M. Grätzel, Low-cost, high efficiency solar cell based on dye-sensitized colloidal TiO2 films, Nature, 353 (1991) 737-740.

[2] M. Grätzel, Photoelectrochemical cells Nature Biotechnology, 414 (2001) 338-344.

[3] M. Wu, T. Ma, Platinum-Free Catalysts as Counter Electrodes in Dye-Sensitized Solar Cells, ChemSusChem, 5 (2012) 1343-1357.

[4] R. Jose, V. Thavasi, S. Ramakrishna, Metal Oxides for Dye-Sensitized Solar Cells, Journal of the American Ceramic Society, 92 (2009) 289-301.

[5] M. Ohta, N. Koumura, K. Hara, S. Mori, Concerted effect of large molecular dyes and bulky cobalt complex redox couple to retard recombination in dye-sensitized solar cells, Electrochemistry Communications, 13 (2011) 778-780.

[6] Y. Fang, J. Zhang, X. Zhou, Y. Lin, S. Fang, "Soggy sand" electrolyte based on COOH-functionalized silica nanoparticles for dye-sensitized solar cells, Electrochemistry Communications, 16 (2012) 10-13.

[7] G.R. Li, F. Wang, J. Song, F.Y. Xiong, X.P. Gao, TiN-conductive carbon black composite as counter electrode for dye-sensitized solar cells, Electrochimica Acta, 65 (2012) 216-220.

[8] K.-M. Lee, W.-H. Chiu, H.-Y. Wei, C.-W. Hu, V. Suryanarayanan, W.-F. Hsieh, K.-C. Ho, Effects of mesoscopic poly(3,4-ethylenedioxythiophene) films as counter electrodes for dye-sensitized solar cells, Thin Solid Films, 518 (2010) 1716-1721.

[9] R. Trevisan, M. Döbbelin, P.P. Boix, E.M. Barea, R. Tena-Zaera, I. Mora-Seró, J. Bisquert, PEDOT Nanotube Arrays as High Performing Counter Electrodes for Dye Sensitized Solar Cells. Study of the Interactions Among Electrolytes and Counter Electrodes, Advanced Energy Materials, 1 (2011) 781-784.

[10] P. Balraju, M. Kumar, M.S. Roy, G.D. Sharma, Dye sensitized solar cells (DSSCs) based on modified iron phthalocyanine nanostructured TiO2 electrode and PEDOT:PSS counter electrode, Synth. Met., 159 (2009) 1325-1331.

[11] G. Yue, J. Wu, Y. Xiao, J. Lin, M. Huang, Z. Lan, Application of Poly(3,4-ethylenedioxythiophene):Polystyrenesulfonate/Polypyrrole Counter Electrode for Dye-Sensitized Solar Cells, The Journal of Physical Chemistry C, 116 (2012) 18057-18063.

[12] J. Wu, Q. Li, L. Fan, Z. Lan, P. Li, J. Lin, S. Hao, High-performance polypyrrole nanoparticles counter electrode for dye-sensitized solar cells, Journal of Power Sources, 181 (2008) 172-176.

[13] S. Cho, S.H. Hwang, C. Kim, J. Jang, Polyaniline porous counter-electrodes for high performance dye-sensitized solar cells, J. Mater. Chem., 22 (2012) 12164.

[14] G.R. Li, J. Song, G.L. Pan, X.P. Gao, Highly Pt-like electrocatalytic activity of transition metal nitrides for dye-sensitized solar cells, Energy & Environmental Science, 4 (2011) 1680.

[15] K.M. Lee, C.Y. Hsu, P.Y. Chen, M. Ikegami, T. Miyasaka, K.C. Ho, Highly porous PProDOT-Et2 film as counter electrode for plastic dye-sensitized solar cells, Physical chemistry chemical physics : PCCP, 11 (2009) 3375-3379.

[16] A. Kaniyoor, S. Ramaprabhu, Thermally exfoliated graphene based counter electrode for low cost dye sensitized solar cells, J. Appl. Phys., 109 (2011) 124308.

[17] P. Poudel, A. Thapa, H. Elbohy, Q. Qiao, Improved performance of dye solar cells using nanocarbon as support for platinum nanoparticles in counter electrode, Nano Energy, 5 (2014) 116-121.

[18] S. Gagliardi, L. Giorgi, R. Giorgi, N. Lisi, T. Dikonimos Makris, E. Salernitano, A. Rufoloni,

Impedance analysis of nanocarbon DSSC electrodes, Superlattices and Microstructures, 46 (2009) 205-208.

[19] J.Y. Lin, C.Y. Chan, S.W. Chou, Electrophoretic deposition of transparent MoS2-graphene nanosheet composite films as counter electrodes in dye-sensitized solar cells, Chemical communications, 49 (2013) 1440-1442.

[20] T.N. Murakami, S. Ito, Q. Wang, M.K. Nazeeruddin, T. Bessho, I. Cesar, P. Liska, R. Humphry-Baker, P. Comte, P.t. Péchy, M. Grätzel, Highly Efficient Dye-Sensitized Solar Cells Based on Carbon Black Counter Electrodes, J. Electrochem. Soc., 153 (2006) A2255.

[21] K. Imoto, K. Takahashi, T. Yamaguchi, T. Komura, J.-i. Nakamura, K. Murata, High-performance carbon counter electrode for dye-sensitized solar cells, Solar Energy Materials and Solar Cells, 79 (2003) 459-469.

[22] Y. Xiao, J. Wu, G. Yue, J. Lin, M. Huang, Z. Lan, Low temperature preparation of a high performance Pt/SWCNT counter electrode for flexible dye-sensitized solar cells, Electrochimica Acta, 56 (2011) 8545-8550.

[23] E. Ramasamy, W.J. Lee, D.Y. Lee, J.S. Song, Spray coated multi-wall carbon nanotube counter electrode for tri-iodide (I3-) reduction in dye-sensitized solar cells, Electrochemistry Communications, 10 (2008) 1087-1089.

[24] S. Iijima, Helical microtubules of graphitic carbon, Nature Biotechnology, (1991) 354 - 356.

[25] H.J. Choi, J.E. Shin, G.-W. Lee, N.-G. Park, K. Kim, S.C. Hong, Effect of surface modification of multi-walled carbon nanotubes on the fabrication and performance of carbon nanotube based counter electrodes for dye-sensitized solar cells, Current Applied Physics, 10 (2010) S165-S167.

[26] W.J. Lee, E. Ramasamy, D.Y. Lee, J.S. Song, Efficient dye-sensitized solar cells with catalytic multiwall carbon nanotube counter electrodes, ACS Appl Mater Interfaces, 1 (2009) 1145-1149.

[27] J.G. Nam, Y.J. Park, B.S. Kim, J.S. Lee, Enhancement of the efficiency of dye-sensitized solar cell by utilizing carbon nanotube counter electrode, Scripta Materialia, 62 (2010) 148-150.

[28] C.-Y. Liu, K.-C. Huang, P.-H. Chung, C.-C. Wang, C.-Y. Chen, R. Vittal, C.-G. Wu, W.-Y. Chiu, K.-C. Ho, Graphene-modified polyaniline as the catalyst material for the counter electrode of a dye-sensitized solar cell, Journal of Power Sources, 217 (2012) 152-157.

[29] S. Hou, X. Cai, H. Wu, Z. Lv, D. Wang, Y. Fu, D. Zou, Flexible, metal-free composite counter electrodes for efficient fiber-shaped dye-sensitized solar cells, Journal of Power Sources, 215 (2012) 164-169.

[30] G. Wang, W. Xing, S. Zhuo, The production of polyaniline/graphene hybrids for use as a counter electrode in dye-sensitized solar cells, Electrochimica Acta, 66 (2012) 151-157.

[31] G. Decher, Fuzzy Nanoassemblies: Toward Layered Polymeric Multicomposites
Science 277 (1997) 1232-1237.

[32] H. Chen, S. Dong, A method to construct polyelectrolyte multilayers film containing gold nanoparticles, Talanta, 71 (2007) 1752-1756.

[33] C.-W. Kuo, T.-C. Wen, Dispersible polyaniline nanoparticles in aqueous poly(styrenesulfonic acid) via the interfacial polymerization route, European Polymer Journal, 44 (2008) 3393-3401.

[34] J. Zhu, J. Wang, F. Lv, S. Xiao, C. Nuckolls, H. Li, Synthesis and self-assembly of photonic materials from nanocrystalline titania sheets, Journal of the American Chemical Society, 135 (2013) 4719-4721.

[35] W. Sun, T. Peng, Y. Liu, W. Yu, K. Zhang, H.F. Mehnane, C. Bu, S. Guo, X.Z. Zhao, Layer-by-layer self-assembly of TiO2 hierarchical nanosheets with exposed {001} facets as an

effective bifunctional layer for dye-sensitized solar cells, ACS Appl Mater Interfaces, 6 (2014) 9144-9149.

[36] E. Detsri, S.T. Dubas, Interfacial polymerization of polyaniline and its layer-bylayer assembly into polyelectrolytes multilayer thin-films, Journal of Applied Polymer Science 128 (2013) 558-565.

[37] J.D. Roy-Mayhew, D.J. Bozym, C. Punckt, I.A. Aksay, Functionalized graphene as a catalytic counter electrode in dye-sensitized solar cells ACS Nano, 4 (2010) 6203-6211.

[38] L. Han, N. Koide, Y. Chiba, A. Isalam, R. Komiya, F. Fuke, Ymanaka, Improvement of efficiency dye-sensitized solar cells by reduction of internal resistanc Appl. Phys. Lett., 86 (2005) 213501-213503.

[39] C. Xu, J. Li, X. Wang, J. Wang, L. Wan, Y. Li, M. Zhang, X. Shang, Y. Yang, Synthesis of hemin functionalized graphene and its application as a counter electrode in dye-sensitized solar cells, Materials Chemistry and Physics 132 (2012) 858-864.

[40] D.W. Zhang, X.D. Li, H.B. Li, S. Chen, Z. Sun, X.J. Yin, S.M. Huang, Graphene-based counter electrode for dye-sensitized solar cells, Carbon, 49 (2011) 5382-5388.

[41] S. Das, P. Sudhagar, V. Verma, D. Song, E. Ito, S.Y. Lee, Y. Kang, W. Choi, Amplifying Charge-Transfer Characteristics of Graphene for Triiodide Reduction in Dye-Sensitized Solar Cells Adv. Funct. Mater., 21 (2011) 3729-3736

[42] G. Wang, W. Xing, S. Zhuo, Nitrogen-doped graphene as low-cost counter electrode for high-efficiency dye-sensitized solar cells, Electrochimica Acta, 92 (2013) 269-275.

[43] B. Lee, D.B. Buchholz, R.P.H. Chang, An all carbon counter electrode for dye sensitized solar cells, Energy & Environmental Science, 5 (2012) 6941.

Table1. Photovoltaic performance of $(CNT^-/CNT^+)_n$ multilayer and Pt-CE based dye-sensitized solar cells (DSSCs).

Counter electrode	J_{sc} (mA/cm^2)	V_{oc}(V)	FF	PCE (%)	$R_s(\Omega)$	$R_{ct}(\Omega)$
$(CNT^-/CNT^+)_1$	16.79	0.68	0.65	7.51	4.2	2
$(CNT^-/CNT^+)_2$	17.05	0.69	0.67	7.97	3.7	1.2
$(CNT^-/CNT^+)_3$	17.67	0.69	0.69	8.43	3.5	0.8
$(CNT^-/CNT^+)_4$	18.03	0.71	0.71	9.13	3.3	0.3
Pt	17.16	0.72	0.68	8.40	4.4	0.96

Fig.1 Schematic illustration of the fabrication procedure of $(CNT^-/CNT^+)_n$ multilayer films on FTO glass-CE.

Fig.2. (a-e) SEM and TEM images of PDADMAC/MWCNT, PANI-PSS/MWCNT and CNT^-/CNT^+ multilayer composite. (f) UV-vis absorption spectra of CNT^-/CNT^+ multilayer deposited on FTO glass with various bilayers. Inset shows a plot of absorbance at 750 nm *vs* bilayer numbers.

Fig.3. (a) Schematic illustration of a DSSC device using the $(CNT^-/CNT^+)_n$ multilayer-CE.
(b) Photocurrent density *vs* voltage of DSSCs from the $(CNT^-/CNT^+)_n$ multilayer-CEs.
(c-f) PCE, FF, V_{oc} and J_{sc} of $(CNT^-/CNT^+)_n$ multilayer-CE, respectively.

Fig.4. Cyclic voltammograms for the $(CNT^-/CNT^+)_n$ multilayer-CE, the electrolyte was acetonitrile solution containing 10 mM LiI, 5 mM I$_2$, and 0.1M LiClO$_4$. Pt electrode is used as auxiliary electrode and Ag/AgCl works as reference electrode, the scan rate is 50 mV s^{-1}.

Fig.5. EIS analysis of $(CNT^-/CNT^+)_n$ multilayer-CE and equivalent circuit models. R_s, R_{ct}, C_{dl} and Z_w are serial resistance, charge-transfer resistance of electrode, double layer capacitance and diffusion impedance, respectively.

Fig.6. (a) Schematic illustration of a DSSC device using the $(CNT^-/CNT^+)_4$ multilayer and Pt-CE.
(b) Photovoltaic performance of $(CNT^-/CNT^+)_4$ multilayer and Pt-CE based DSSCs.(c) CV for the $(CNT^-/CNT^+)_4$ multilayer and Pt-CE. (d) EIS analysis of $(CNT^-/CNT^+)_4$ multilayer and Pt-CE.
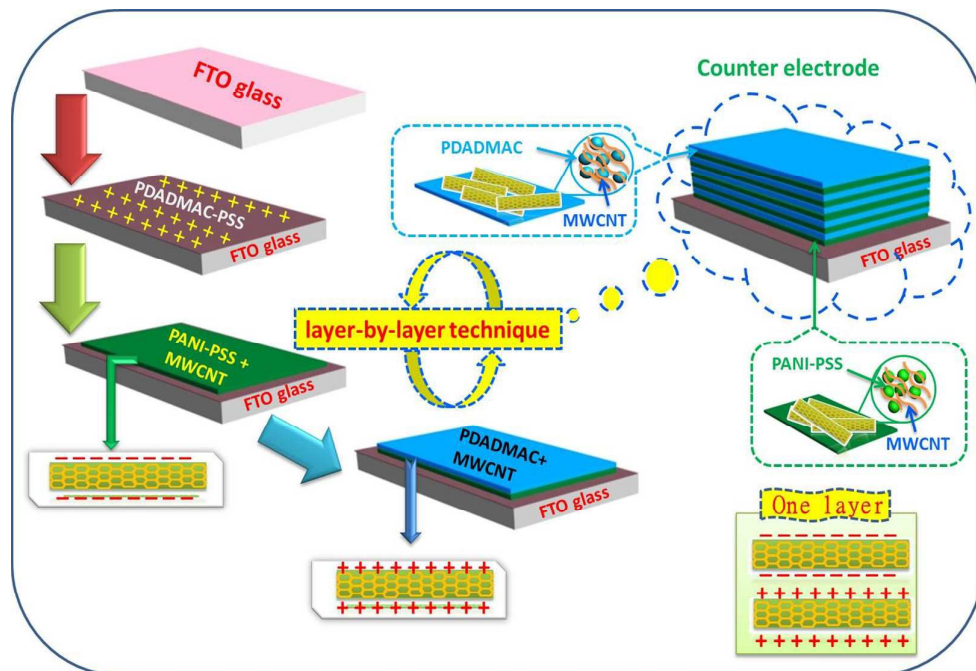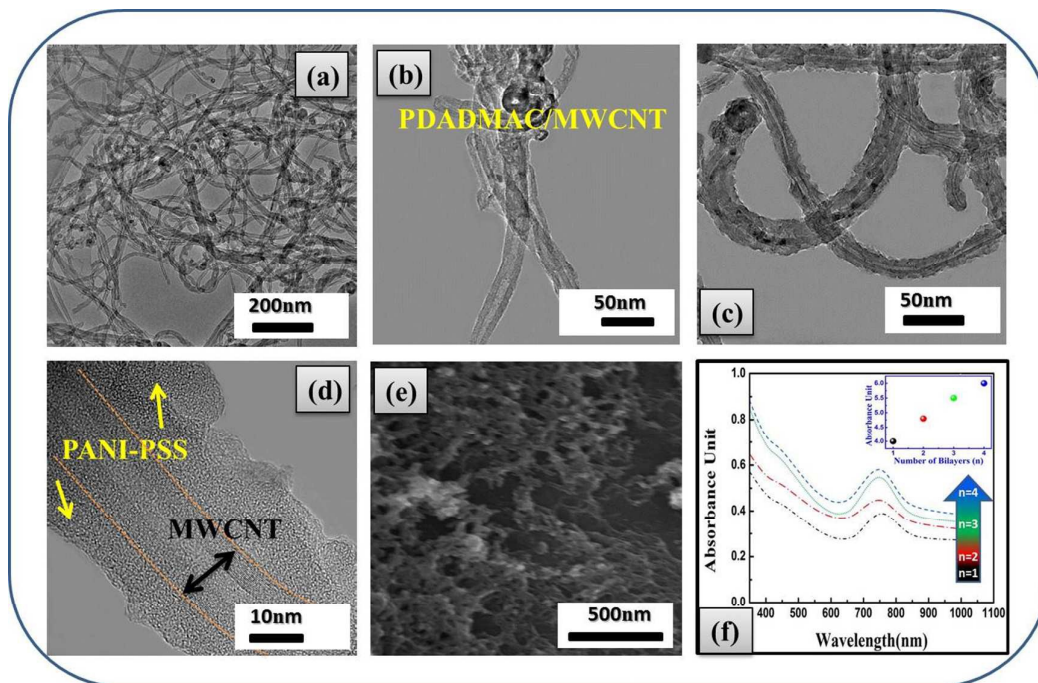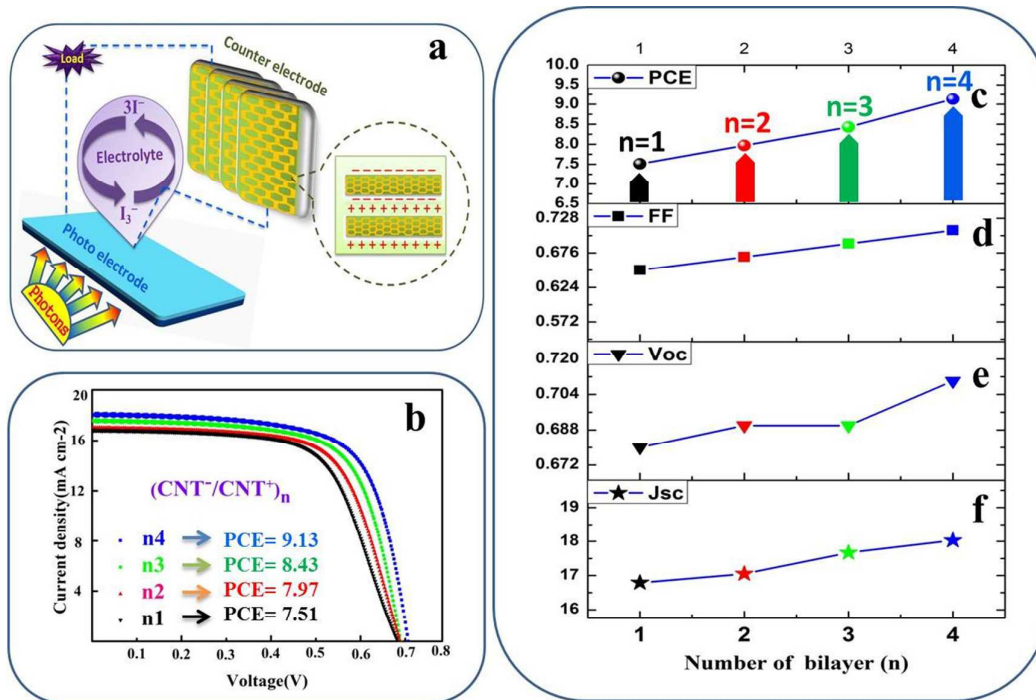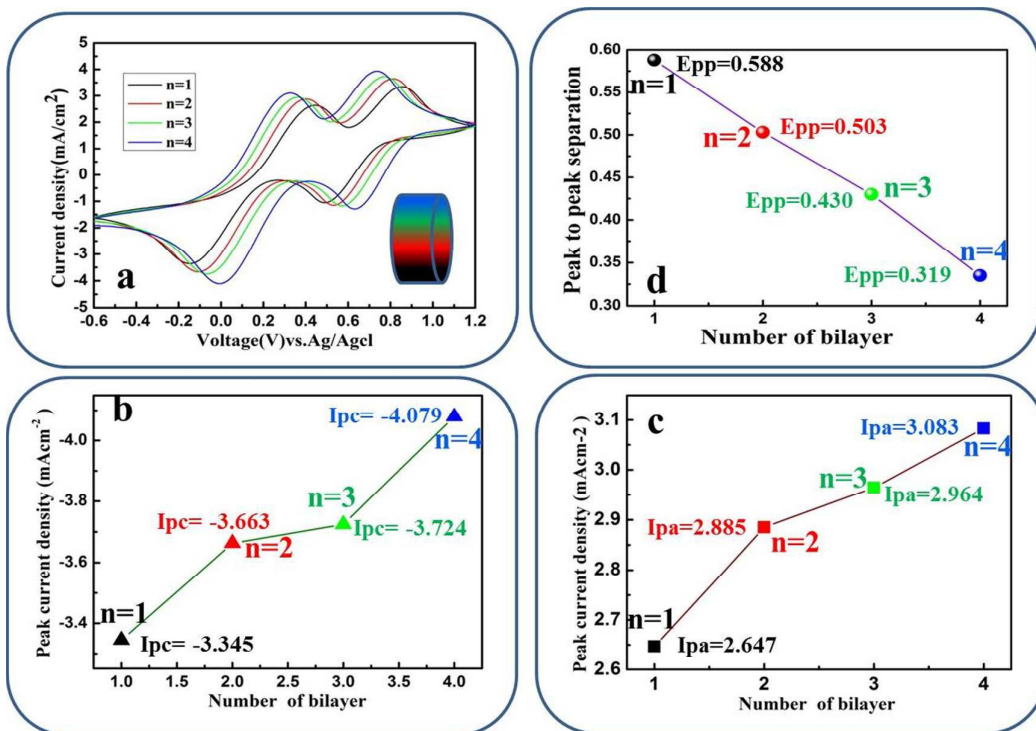
Fig.1

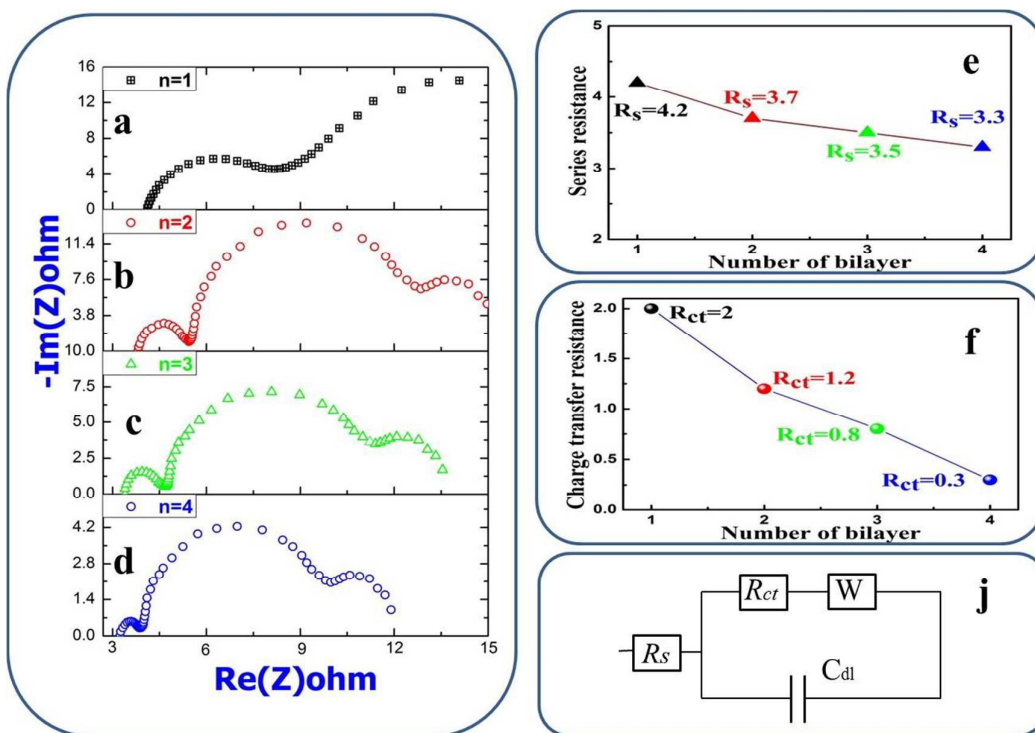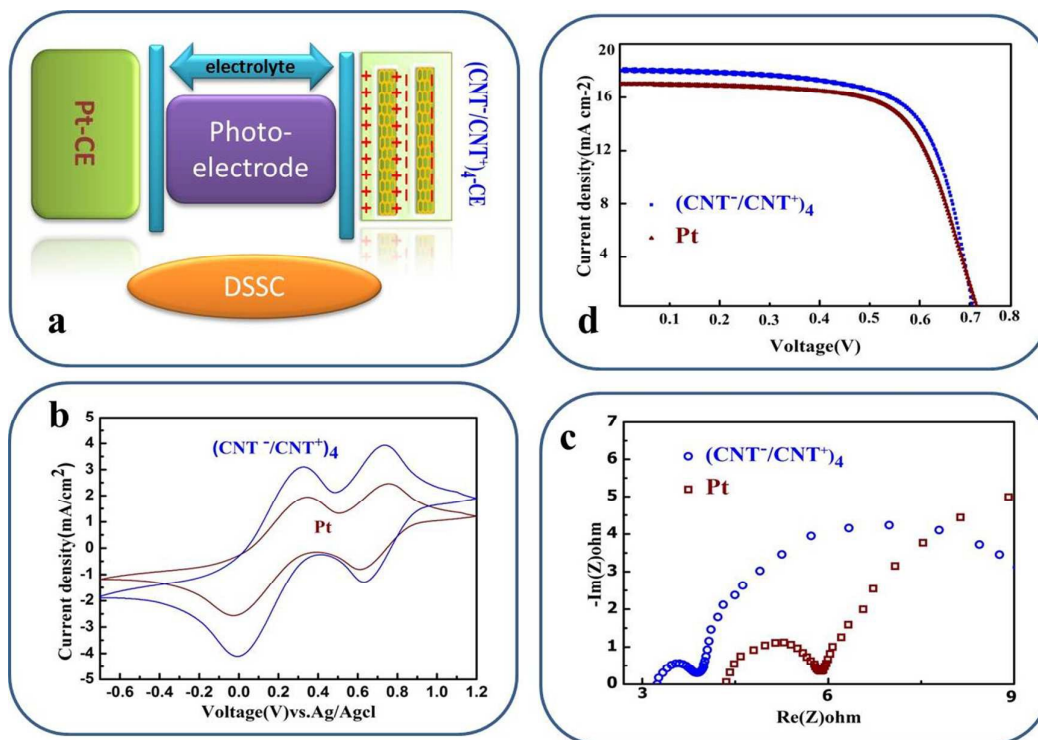
Fig.2

Fig. 3

Fig. 4

Fig. 5

Fig. 6

Layer-by-layer deposition of CNT⁻ and CNT⁺ hybrid films for platinum free counters electrodes of dye-sensitized-solar-cells